Supplementary Material: Climate and landscape jointly control Europe's hydrology

Julia Maria Rudlang[1], Thiago V.M. do Nascimento[2,3], Ruud van der Ent[1], Fabrizio Fenicia[2], and Markus Hrachowitz[1]

[1]Department of Water Management, Faculty of Civil Engineering and Geosciences, Delft University of Technology, Delft, the Netherlands
[2]Eawag: Swiss Federal Institute of Aquatic Science and Technology, Dübendorf, Switzerland
[3]Department of Geography, University of Zurich, Zurich, Switzerland

Correspondence: Julia Maria Rudlang (J.M.Rudlang@tudelft.nl)

S1 Circular statistics

The signatures and attributes related to the timing, like the half-flow day ($H_{\mathrm{t(HFD)}}$) or the day of year when the first water deficit occurs ($C_{\mathrm{t(WD_{first})}}$) had to be decomposed into their respective sine and cosine components to account for the circularity in the year when using k-means clustering and Random Forest classification model. Thus, both the timing and inter-annual variance of the timing were calculated using the concept of circular statistics (Parajka et al., 2010; Blöschl et al., 2017; Berghuijs et al., 2025). The normalised day of year, t_{norm} (ranging from 0 to 1), was mapped onto the unit circle using two dimensionless circular coordinates:

$t_{SA} = \cos(2\pi\, t_{norm})$ (spring-autumn axis),

from which the corresponding sine and cosine components:

$t_{WS} = \sin(2\pi\, t_{norm})$ (winter-summer axis)

This decomposition ensures that dates near the year boundary (e.g, December 31st and January 2nd) are represented as nearby points on the circle, allowing for a correct computation of mean timing. The circular mean vector $(\overline{t_{SA}}, \overline{t_{WS}})$ was then converted back to day of year using: $t_{doy} = (365.25/2\pi) * \mathrm{atan2}(\overline{t_{SA}}, \overline{t_{WS}})$, producing an unambiguous average day of the year. In this mapping, $t_{WS} = -1$ corresponds approximately to January 1st and $t_{WS} = +1$ to July 1st, while $t_{SA} = +1$ corresponds approximately to April 1st and $t_{SA} = -1$ to October 1st.

S1.1 Timing

For each hydrological signature and climate attribute with a seasonal timing component, the timing of the signature or attribute was defined as the day of year (DOY) at which the mean annual cycle reached its maximum or minimum or first or last occurrence, depending on the signature definition (e.g., timing of high flow, timing of low flow, first occurrence of water deficit). This yields a single day of the year, representing the timing, ranging from 1 to 365 (or 366 in leap years).

Because timing is inherently circular (DOY 1 follows DOY 365), each timing value *t* was expressed in its angular form:

$$\theta = \frac{2\pi t}{365.25},$$

from which the corresponding sine and cosine components:

$$t_{WS} = \sin(\theta), \quad t_{SA} = \cos(\theta).$$

These circular representations were used to ensure consistency across timing signatures when using k-means clustering and Random Forest classification models, and allowed transformation back to the DOY domain when needed. The angle was converted back to DOY using:

$$t = \frac{365.25}{2\pi}\,\mathrm{atan2}(t_{WS}, t_{SA}),$$

with wrap-around corrections applied to keep t within the range of [0, 365.25].

S1.2 Inter-annual variability of timing

To quantify inter-annual variability in timing, we extracted the annual timing value of each signature and attribute for every individual year of record. For a catchment with *n* years of data, resulted in a vector of annual timing values: $t_1, t_2, ..., t_n$ (DOY).

Each annual timing value was converted to an angular direction on the unit circle:

$$\theta_i = \frac{2\pi t_n}{365.25}.$$

For which we computed the mean sine and cosine components:

$$\overline{t_{n,WS}} = \frac{1}{n}\sum_{i=1}^{n} \sin(\theta_i), \quad \overline{t_{n,SA}} = \frac{1}{n}\sum_{i=1}^{n} \cos(\theta_i),$$

The circular mean timing was obtained as:

$$\overline{\theta} = \mathrm{atan2}(\overline{t_{n,WS}}, \overline{t_{n,SA}}).$$

The concentration parameter, or mean resultant length, was calculated as:

$$R = \sqrt{\overline{t_{n,WS}}^2 + \overline{t_{n,SA}}^2},$$

with circular variance defined as: $V = 1 - R$.

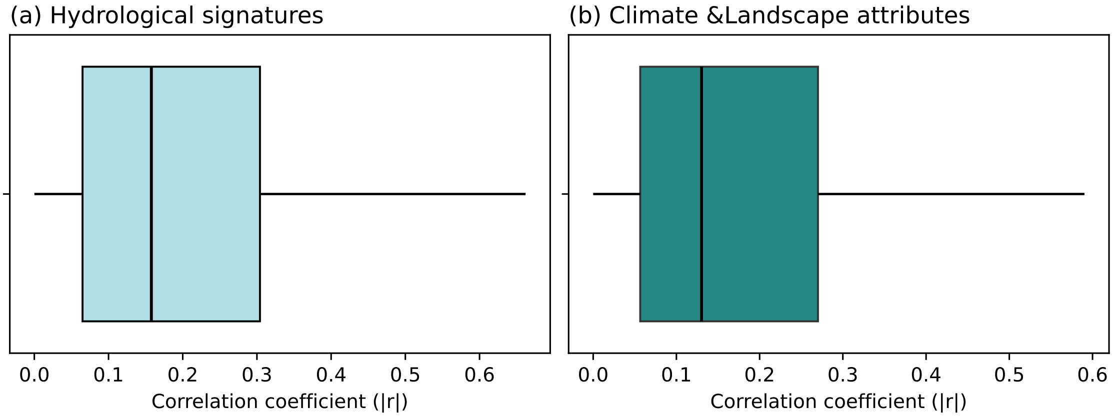

Figure S1. Distribution of correlation values between hydrological signatures and climate and landscape attributes. (a) boxplots of the correlations for 40 hydrological signatures. (b) boxplots of the correlations for 84 climate and landscape attributes. These plots illustrate the range and variability of relationships between catchment characteristics and hydrological responses.

S2 Hydrological Signatures

Table S1: Overview of the hydrological signatures

Category	Variable Name	Unit	Description
Magnitude			
	H_{Q}	mm d^{-1}	Mean daily streamflow.
	H_{Q_5}	mm d^{-1}	Q_5 is the 5% flow quantile, representing low flows.
	$H_{Q_{95}}$	mm d^{-1}	Q_{95} is the 95% flow quantile, representing high flows.
Frequency			
	$H_{f(\mathrm{Q}_H)}$	d yr^{-1}	Frequency of high flows, when Q $>$ 9 the median daily flow.
	$H_{f(\mathrm{Q}_L)}$	d yr^{-1}	Frequency of low flows, when Q $<$ 0.2 times the median daily flow.
	$H_{f(\mathrm{Q}_Z)}$	d yr^{-1}	Frequency of zero flow, where days with Q $= 0$.
Duration			
	$H_{D(\mathrm{Q}_H)}$	d	Average duration of high flow events of consecutive days $>$ 9 times the median daily flow.
	$H_{D(\mathrm{Q}_L)}$	d	Average duration of flow flow events of consecutive days of $<$ 0.2 times the median daily flow.
Timing			

Category	Variable Name	Unit	Description
	$H_{t(\text{HFD})_{WS}}$	-	The winter-summer component of the timing of the half-flow day, which is the day when the cumulative daily streamflow is half the annual streamflow.
	$H_{t(\text{HFD})_{SA}}$	-	The spring-autumn component of the timing of the half-flow day, which is the day when the cumulative daily streamflow is half the annual streamflow.
	$H_{t(\text{Q}_H)_{WS}}$	-	The winter-summer component of the timing of high flow.
	$H_{t(\text{Q}_H)_{SA}}$	-	The spring-autumn component of the timing of high flow.
	$H_{t(\text{Q}_L)_{WS}}$	-	The winter-summer component of timing of low flow.
	$H_{t(\text{Q}_L)_{SA}}$	-	The spring-autumn component of the timing of low flow.
Seasonality			
	$H_{N(\text{Q}_H\text{-Q}_L)}$	d	Days between highest and lowest flow.
	H_{FDC}	-	Slope of the flow duration curve. Given as: $\frac{ln(Q_{33\%})-ln(Q_{66\%})}{(0.66-0.33)}$ (Sawicz et al., 2011).
	H_{RLD}	d^{-1}	Rising limb density, which is the number of rising peaks divided by the total time the hydrograph is rising, calculated as: $RLD = \frac{N_{RL}}{T_R}$, where N_{RL} is the number of rising limbs and T_R is the total time rising (Sawicz et al., 2011).
	H_{FLD}	d^{-1}	Falling limb density, which is the number of falling peaks divided by the total time the hydrograph is falling, calculated as: $FLD = \frac{N_{FL}}{T_F}$, where N_{FL} is the number of falling limbs and T_F is the total time falling (Sawicz et al., 2011).
	H_{RBI}	-	The Richard-Baker Flashiness Index, which measures oscillations in discharge relative to total discharge given as: $R-BIndex = \frac{\Sigma_{i=1}^{n}\lvert q_i-qi-1\rvert}{\Sigma_{i=1}^{n}q_i}$ (Baker et al., 2004).
	H_{GC}	-	Mean Gini coefficient, which is a measure of dispersion. It is computed after the sorted and normalised daily streamflow values (x_i) as:$G = \frac{2\sum_{i=1}^{n} i\,x_{(i)}}{n\sum_{i=1}^{n} x_{(i)}} - \frac{n+1}{n}$ where n is the number of observations and the Gini coefficient, G, varies between 0 and 1, representing a non-uniform to uniform flow.

Category	**Variable Name**	**Unit**	**Description**
	$H_{\mathrm{R(Parde)}}$	-	The range of the Parde coefficients, where the Parde coefficient is expressed as: $PK_i = \frac{Q_i}{Q_A}$. Where PK_i is the Parde coefficient for month i, Q_i is the mean monthly streamflow over all years, and Q_A is the mean annual streamflow over all years. The range is thus calculated as: $PK_{max} - PK_{min}$ (Blöschl et al., 2013).
	$H_{\mathrm{AC_1}}$	-	The autocorrelation with 1 day lag, calculated as: $AC = \frac{\Sigma(Q_i-\overline{Q})(Q_{i+1}-\overline{Q}}{\Sigma(Q_i-\overline{Q})^2}$, where Q_i is the streamflow at time step i and $\overline{Q}$ is the average streamflow (Euser et al., 2013).
	$H_{\mathrm{AC_{30}}}$	-	The autocorrelation with 30 days lag, calculated as: $AC = \frac{\Sigma(Q_i-\overline{Q})(Q_{i+30}-\overline{Q}}{\Sigma(Q_i-\overline{Q})^2}$, where Q_i is the streamflow at time step i and $\overline{Q}$ is the average streamflow (Euser et al., 2013).
	H_{BFI}	-	The baseflow index, which is the ratio of mean daily baseflow to mean daily discharge is computed by hydrograph separation using digital filter: $q_f(i) = \begin{cases} \alpha q_f(i-1) + \frac{1+\alpha}{2}[q(i) - q(i-1) & \text{for} q_f(i) > 0 \\ 0 & \text{otherwise} \end{cases}$ $q_b(i) = q(i) - q_f(i)$, where $q_f(i)$ is the quick flow response at the i^{th} sampling instant, $q(i)$ is the original streamflow at i^{th} sampling instant, $q_b(i)$ is the baseflow at the i^{th} sampling instant and α is the filter parameter (Ladson et al., 2013).
	H_{CV}	-	Coefficient of variation of the daily streamflow.
Inter-annual Variance			
	$H_{\mathrm{V,Q}}$	$(\mathrm{mm\ d^{-1}})^2$	Inter-annual variance of daily streamflow.
	H_{V,Q_5}	$(\mathrm{mm\ d^{-1}})^2$	Inter-annual variance of Q_5.
	$H_{\mathrm{V,Q_{95}}}$	$(\mathrm{mm\ d^{-1}})^2$	Inter-annual variance of Q_{95}.
	$H_{\mathrm{V},f(\mathrm{Q}_H)}$	$(\mathrm{d\ yr^{-1}})^2$	Inter-annual variance of the frequency of high flow events.
	$H_{\mathrm{V},f(\mathrm{Q}_L)}$	$(\mathrm{d\ yr^{-1}})^2$	Inter-annual variance of the frequency of low flow events.
	$H_{\mathrm{V},f(\mathrm{Q}_Z)}$	$(\mathrm{d\ yr^{-1}})^2$	Inter-annual variance of frequency of zero flow.
	$H_{\mathrm{V},D(\mathrm{Q}_H)}$	d^2	Inter-annual variance of the duration of high flow events.
	$H_{\mathrm{V},D(\mathrm{Q}_L)}$	d^2	Inter-annual variance of the duration of low flow events.
	$H_{\mathrm{V},t(\mathrm{HFD})}$	d^2	Inter-annual variance of the half-flow day.
	$H_{\mathrm{V},t(\mathrm{Q}_H)}$	d^2	Inter-annual variance of timing of highest flow event.
	$H_{\mathrm{V},t(\mathrm{Q}_L)}$	d^2	Inter-annual variance of timing of lowest flow event.

Category	Variable Name	Unit	Description
	$H_{\mathrm{V,N(Q_H\text{-}Q_L)}}$	d^2	Inter-annual variance of days between highest and lowest flow.
	$H_{\mathrm{V,FDC}}$	-	Inter-annual variance of the slope of the flow duration curve.
	$H_{\mathrm{V,GC}}$	-	Inter-annual variance of the Gini coefficient.
	$H_{\mathrm{V,R(Parde)}}$	-	Inter-annual variance of the range of the Parde coefficients.

S3 Climate and landscape attributes

Table S2: Climate and landscape attributes

Category	Variable Name	Unit	Description
Climate			
Magnitude			
	$C_{\mathrm{E_P}}$	mm d^{-1}	Mean potential evaporation (E_P), estimated using: $ET_0 = 0.0023\,(T_{\mathrm{mean}}+17.8)\,(T_{\mathrm{max}}-T_{\mathrm{min}})^{0.5}\,R_{athe}$ from Hargreaves and Samani (1982).With T as temperature and $R_a the$ as the extraterrestrial radiation.
	$C_{\mathrm{E_a}}$	mm d^{-1}	Mean actual evaporation (Ea), approximated from scaling Ep as $E_a(i) = E_P(i) * \frac{\overline{E_a}}{E_P}$, where i is the daily timestep and $\overline{E_a}$ is derived from the long-term water balance: $\overline{E_a} = \overline{P} - \overline{Q}$.
	C_{T}	°C	Mean temperature. Daily time series from E-OBS.
	$C_{\mathrm{P_L}}$	mm d^{-1}	Mean liquid water as the sum of rainfall and snowmelt ($P_L = P_R + P_M$). The components are derived from a simple degree-day snow model in section S4.
	C_{P_M}	mm d^{-1}	Mean water input from snowmelt, derived from a simple degree-day snow model in section S4.
	$C_{\mathrm{WD}_{max}}$	mm	Median duration of long-term water deficit, derived from precipitation (P) and actual evaporation (E_a) (section S6).
	$C_{F(\mathrm{Snow})}$	-	Median annual fraction of precipitation falling as snow.
Frequency			
	$C_{f(\mathrm{P}_{LH})}$	d yr^{-1}	Frequency of high P_L events, when $P_L > 5$ times the median daily P_L.

Category	Variable Name	Unit	Description
	$C_{f(\mathrm{P}_{LL})}$	d yr^{-1}	Frequency of low P_L events, when $P_L < 1$ mm d^{-1}.
Duration			
	$C_{N(\mathrm{P}_L)}$	d	Median annual number of days when P_L occurs.
	$C_{D(\mathrm{P}_{LH})}$	d	Average duration of periods with consecutive high P_L events.
	$C_{D(\mathrm{P}_{LL})}$	d	Average duration of periods with consecutive low P_L events.
	$C_{D(\mathrm{WD})}$	d	Median duration of water deficit.
	$C_{\mathrm{D}(\mathrm{WD}_{\mathrm{max}})}$	d	Median of the annual longest periods of water deficit.
	$C_{\mathrm{N}(\mathrm{WD})}$	d	Median annual days with water deficit.
	$C_{D(\mathrm{SnowC}_{\mathrm{max}})}$	d	Median duration of the longest annual snow cover, derived from the snow storage (see section S5).
	$C_{D(\mathrm{SnowC})}$	d	Median of the annual mean duration of snow cover, when there is a positive snow storage (see section S5).
Timing			
	$C_{t(\mathrm{P}_{L,max})_{WS}}$	-	The winter-summer component of the timing of the highest P_L event. See section on circular statistics for calculation (see section S1)
	$C_{t(\mathrm{P}_{L,max})_{SA}}$	-	The spring-autumn component of the timing of the highest P_L event. See section on circular statistics for calculation (see section S1)
	$C_{t(\mathrm{WD}_{\mathrm{first}})_{WS}}$	-	The winter-summer component of the timing of the first annual water deficit.
	$C_{t(\mathrm{WD}_{\mathrm{first}})_{SA}}$	-	The spring-autumn component of the timing of the first annual water deficit.
	$C_{t(\mathrm{WD}_{\mathrm{last}})_{WS}}$	-	The winter-summer component of the timing of the last annual water deficit.
	$C_{t(\mathrm{WD}_{\mathrm{last}})_{SA}}$	-	The spring-autumn component of the timing of the last annual water deficit.
	$C_{t(\mathrm{WD}_{\mathrm{max}})_{WS}}$	-	The winter-summer component of the timing of the annual maximum water deficit.
	$C_{t(\mathrm{WD}_{\mathrm{max}})_{SA}}$	-	The spring-autumn component of the timing of the annual maximum water deficit.
Seasonality			

Category	Variable Name	Unit	Description
	C_{AI}	-	Aridity Index, computed as: $AI = \frac{\overline{P}}{\overline{Ep}}$.
	$C_{R(\mathrm{T})}$	°C	Temperature range of long-term mean annual maximum and minimum temperature.
	$C_{\phi(E_P)}$	-	Seasonality and timing of potential evaporation, derived from precipitation and temperature time series from E-OBS and computed as in equation 13 from Woods (2009): $f_s(\overline{T}^*, \delta_P^*) = \frac{1}{2} - \frac{sin^{-1}(\overline{T}^*)}{\pi} - \frac{\delta_P^*}{\pi}\sqrt{1-\overline{T}^{*2}}$, where $\overline{T}^*$ is the dimensionless mean temperature and the dimensionless δ_P^* that summarises magnitude of seasonal variation of precipitation and its temporal distribution relative to temperature..
	$C_{\phi(\mathrm{P})}$	-	Seasonality and timing of precipitation adapted after equation 13 from Woods (2009).
	$C_{\Delta\phi(P,E_P)}$	-	Difference in seasonal timing between potential evaporation and precipitation, describing whether E_P peaks before or after P in the annual cycle.
	$C_{I(\mathrm{P}_L)}$	mm yr^{-1}	Median annual intensity of P_L.
	$C_{I(\mathrm{P}_M)}$	mm yr^{-1}	Median annual intensity of P_M.
	$C_{S_R(\mathrm{WD}_{max})}$	-	Median of the rising slope of the maximum water deficit.
	$C_{S_D(\mathrm{WD}_{max})}$	-	Median of the declining slope of the maximum water deficit.
Inter-annual Variance			
	C_{V,E_P}	(mm d^{-1})^2	Inter-annual variance of potential evaporation.See section on circular statistics for calculation (S1).
	C_{V,E_A}	(mm d^{-1})^2	Inter-annual variance of actual evaporation.
	$C_{\mathrm{V},\mathrm{P}_L}$	(mm d^{-1})^2	Inter-annual variance of P_L.
	$C_{\mathrm{V},\mathrm{P}_M}$	(mm d^{-1})^2	Inter-annual variance of P_M.
	$C_{\mathrm{V},\mathrm{WD}_{max}}$	mm^2	Inter-annual variance of the maximum water deficit.
	$C_{\mathrm{V},\mathrm{F(Snow)}}$	-	Inter-annual variance of fraction of precipitation falling as snow.
	$C_{\mathrm{V},\mathrm{P_S}}$	(mm d^{-1})^2	Inter-annual variance of snowfall.
	$C_{\mathrm{V},N(\mathrm{P}_L)}$	d^2	Inter-annual variance of days with P_L.

Category	Variable Name	Unit	Description
	$\mathrm{C}_{\mathrm{V},\,\mathrm{N(WD)}}$	d^2	Inter-annual variance of the annual days with water deficit.
	$C_{\mathrm{V},\,t(\mathrm{P}_{L,\,max})}$	d^2	Inter-annual variance of the doy with maximum P_L.
	$C_{\mathrm{V},\,t(\mathrm{WD_{first}})}$	d^2	Inter-annual variance of doy timing of first water deficit.
	$C_{\mathrm{V},\,t(\mathrm{WD_{last}})}$	d^2	Inter-annual variance of doy timing of last water deficit.
	$C_{\mathrm{V},\,t(\mathrm{WD_{max}})}$	d^2	Inter-annual variance of circular doy timing of maximum water deficit.
Vegetation, Static			
Magnitude			
	$V_{F(\mathrm{Forest})}$	-	Mean fraction of forest cover aggregated from CORINE for the years of 1990, 2000, 2006, 2012, 2018.
	$V_{F(\mathrm{Shrub})}$	-	Mean fraction of shrub cover aggregated from CORINE for the years of 1990, 2000, 2006, 2012, 2018.
	$V_{F(\mathrm{Open})}$	-	Mean fraction of open areas aggregated from CORINE for the years of 1990, 2000, 2006, 2012, 2018.
	$V_{F(\mathrm{Wetland})}$	-	Mean fraction of wetland aggregated from CORINE for the years of 1990, 2000, 2006, 2012, 2018.
	$V_{F(\mathrm{TC})}$	-	Mean fraction of tree cover from MODIS.
Seasonality			
	V_{LAI}	-	Median LAI for the period 2001-2022 from MODIS
	V_{NDVI}	-	Median NDVI for the period 2001-2022 from MODIS
Vegetation, Dynamic			
Seasonality			
	$V_{R(\mathrm{LAI_{Parde}})}$	-	Range of Parde coefficients calculated with LAI from MODIS.
	$V_{R(\mathrm{NDVI_{Parde}})}$	-	Range of Parde coefficients calculated with NDVI from MODIS.
Inter-annual Variance			
	$V_{\mathrm{V},\,\mathrm{LAI}}$	-	Inter-annual variance of the median LAI from MODIS.
	$V_{\mathrm{V},\,\mathrm{NDVI}}$	-	Inter-annual variance of the median NDVI from MODIS.

Category	Variable Name	Unit	Description
Soi, Geology, Topography			
Magnitude			
	$S_{F(\mathrm{SG})}$	-	Mean sand and gravel fraction aggregated from the European Soil Database Derived data (ESDD).
	$S_{F(\mathrm{SC})}$	-	Mean silt and clay fraction aggregated from the European Soil Database Derived data (ESDD)
	$S_{F(\mathrm{OC})}$	-	Median soil organic content fraction aggregated from the European Soil Database Derived data (ESDD)
	S_{TWAC}	mm	Median soil total water content from the European Soil Database Derived data (ESDD)
	S_{SBD}	g cm^{-3}	Median soil bulk density from the European Soil Database Derived data (ESDD)
	S_{RD}	cm	Median soil root depth from the European Soil Database Derived data (ESDD)
	$G_{F(\mathrm{SS})}$	-	Mean Sandstone fraction aggregated from the International Hydrogeological Map of Europe (IHME).
	$G_{F(\mathrm{MS})}$	-	Mean Mudstones fraction aggregated from the International Hydrogeological Map of Europe (IHME).
	$G_{F(\mathrm{C})}$	-	Mean Carbonates fraction aggregated from the International Hydrogeological Map of Europe (IHME).
	$G_{F(\mathrm{LP})}$	-	Mean low permeable stones fraction aggregated from the International Hydrogeological Map of Europe (IHME).
	$G_{F(\mathrm{Perm}_{VL})}$	-	Mean Very Low Permeability fraction aggregated from the International Hydrogeological Map of Europe (IHME).
	$G_{F(\mathrm{Perm}_{L})}$	-	Mean Low Permeability fraction aggregated from the International Hydrogeological Map of Europe (IHME).
	$G_{F(\mathrm{Perm}_{M})}$	-	Mean Medium Permeability fraction aggregated from the International Hydrogeological Map of Europe (IHME).
	$G_{F(\mathrm{Perm}_{H})}$	-	Mean High Permeability fraction aggregated from the International Hydrogeological Map of Europe (IHME).
	G_{BD}	m	Mean depth to the bedrock Pelletier et al. (2016).

Category	Variable Name	Unit	Description
	T_{Elev}	m	Mean elevation from MERIT-Hydro.
	$T_{R(\text{Elev})}$	m	Mean elevation range (max - min elevation).
	$T_{F(\text{A}_F)}$	-	Mean flat area fraction, considered the percentage of area with slope $< 3°$ from MERIT-Hydro.
	$T_{F(\text{A}_S)}$	-	Mean steep area fraction, considered the percentage of area with slope $> 15°$ from MERIT-Hydro.
	T_{ER}	-	Mean elongation ratio from MERIT-Hydro.
	T_{DD}	$1000\,\text{km}\,\text{km}^{-2}$	Drainage density, ratio of lengths of streams and the catchment area from MERIT-Hydro.
Anthropogenic			
Magnitude			
	$A_{F(\text{AS})}$	-	Mean fraction of artificial surfaces from CORINE.
	$A_{F(\text{Agri})}$	-	Mean fraction of agricultural areas from CORINE.
	A_{Irr}	-	Median area equipped for irrigation per catchment area. 10/5-year resolution total area equipped for irrigation (period from 1990 - 2005) from AEI EARTHSTAT IR product from HID.
	$A_{\text{ResStorage}}$	mm	Reservoir storage per catchment area from Georeferenced global Dams and Reservoirs.
	A_{Lake_A}	-	Lake area per catchment area. No distinction is made between man-made and natural lakes and dams from HydroLakes.

S4 Snow model

The snow model is based on the degree-day method (Bergstrom, 1975; Gao et al., 2017; Van Oorschot et al., 2024) and relies on input data from catchment precipitation and temperature as daily time series from the E-OBS dataset, as well as elevation data from MERIT-Hydro. Based on the elevation data, individual elevation zones for each catchment can be determined, which helps decide the temperature differences in the catchment. Ultimately, to decide whether precipitation is falling as rain or snow. The elevation zone temperature is calculated like this:

$$T_z(t) = T_a(t) + \lambda \Delta H, \tag{1}$$

where T_a (°C) is the catchment average temperature, λ is the lapse rate of 0.00064°C/m andΔH (m) is the difference in elevation between the zones and the mean elevation. For each elevation zone (z), the daily P_R and P_S were calculated:

$$P_{R,z}(t) = \begin{cases} P(t) & \text{if } T_z(t) > Tt \\ 0 & \text{if } Tz(t) < Tt \end{cases} \tag{2}$$

$$P_{S,z}(t) = \begin{cases} P(t) & \text{if } T_z(t) < Tt \\ 0 & \text{if } Tz(t) > Tt \end{cases} \tag{3}$$

where threshold temperature is TT = -1 °C.

Snowmelt occurs when the temperature is above the TT threshold, and is calculated like this:

$$P_{M,z}(i) = min(S_{s,z}(i), MF * (T_z(i) - TT)) \tag{4}$$

where MF is the degree day factor set at 2.5 °C and $S_{s,z}$ is the snow storage at the elevation zone, and is calculated like this:

$$S_{s,z}(i) = max(0, S_{s,z}(i) - P_M(i) \tag{5}$$

To arrive at a single daily value for precipitation falling as rain (P_R, mm d^{-1}), precipitation falling as snow (P_S, mm d^{-1}), and the amount of snowmelt (P_M, mm d^{-1}), is calculated at each elevation zone (z) and then aggregated.

S5 Snow storage

The overall daily snow storage (mm d^{-1}), $S_s(i)$ for each catchment was calculated as follows:

$$S_s(i) = \begin{cases} 0, & \text{if day(i) = 1 and month(i) = 9} \\ max(0,\, P_S(i) + S_s(i-1) - P_M(i)) & \end{cases} \tag{6}$$

The storage was forced to be set to 0 each September, because for some catchments, the snow storage would accumulate indefinitely. The reason for this is most likely because the degree-day model is not accurate enough, as it is different at what temperatures the snowpack will start to melt, etc. By forcing a reset, the seasonal signal is preserved.

S6 Water deficit

The water deficit was calculated based on the input from actual evaporation, which is approximated with downscaling from potential evaporation (see Table.**??**). The water deficit is then calculated as:

$$SD_t = \begin{cases} 0, & \text{if day}(i) = 1 \text{and month}(i) = 3 \\ min(0,\; SD_{i-1} + P_i - E_{a,i}) & \end{cases} \tag{7}$$

with

$$SD_0 = min(0, P_0 - E_{a,0}) \tag{8}$$

When calculating the water deficit, there are some years with missing data, as explained in the data selection procedure. To avoid having the nan values propagate into the next year's calculation, if a nan was encountered, the previous step was set to zero so the calculation could continue. The reasoning to do so was that when working with the signatures of water deficit, it is the length and the duration of the deficit that are important, so if it is nan or zero, it will not be counted anyway. Each year, when on average most of the catchment converged to zero, the number was set to zero regardless, because it is not realistic that it will never reach zero. The reason for this was that some catchments never reached zero, which might be that there are other factors drawing water out of the catchment that we are not able to account for. It could also be that the approximation for actual evaporation is not good enough for the calculation.

S7 Random Forest classification model

The Random Forest classification model =RandomForestClassifier(n_estimators=494, max_depth=10, min_samples_split=3, min_samples_leaf=13, min_weight_fraction_leaf=0.0, class_weight='balanced', n_jobs=-1, random_state=42)

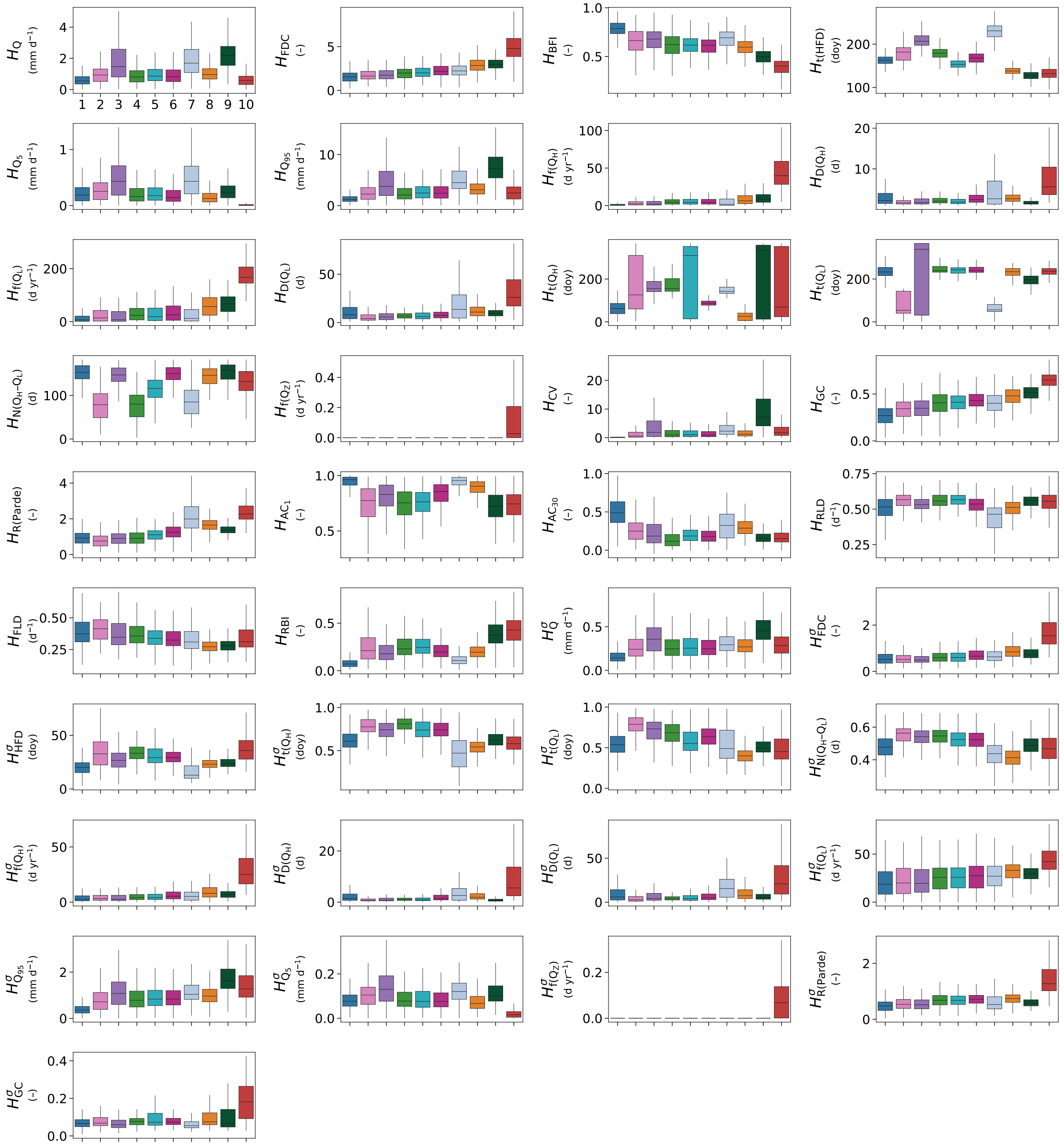

Figure S2. Distribution of 37 hydrological signatures across hydrological response types (HRTs) shown as boxplots. Note that 40 hydrological signatures were used in the k-means clustering; for visualisation purposes, timing signatures are presented as the day of year (DOY), combining their winter–summer and spring–autumn components. Inter-annual variance signatures are shown as standard deviation for easier interpretability.

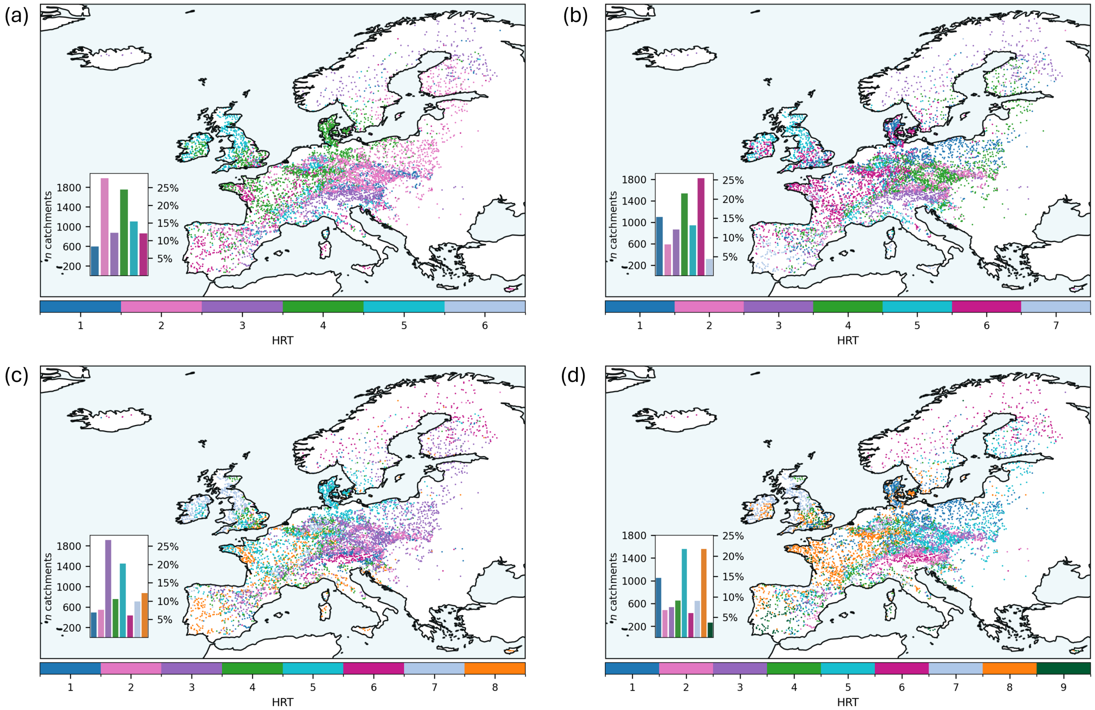

Figure S3. Classification of 7175 catchments into (a) 6 hydrological response types (HRTs), (b) 7 HRTs, (c) 8 HRTs and (d) 9 HRTs based on 40 hydrological signatures. The HRTs are ordered by increasing flow duration curve slopes.

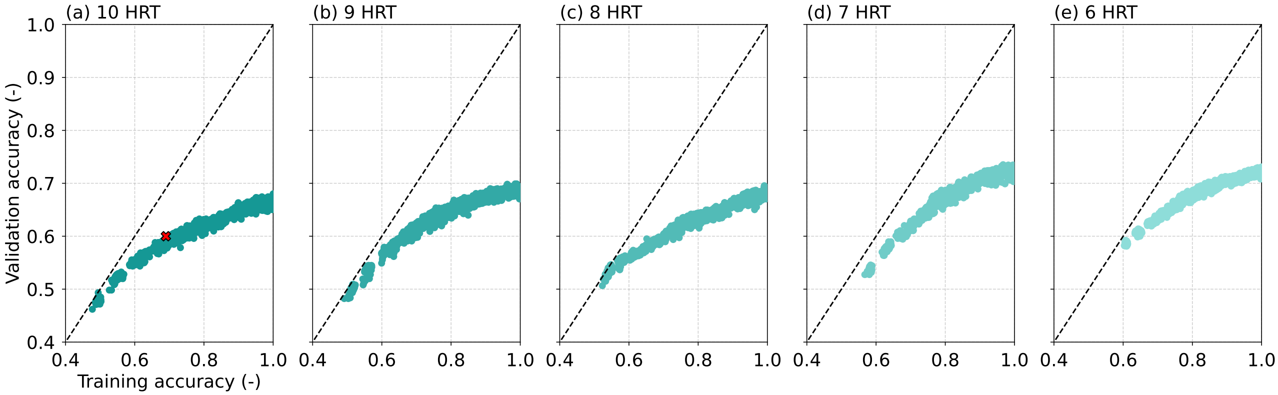

Figure S4. Panels (a)–(e) show validation accuracy versus testing accuracy for random forest classification models predicting 10, 9, 8, 7, and 6 hydrological response types (HRTs), respectively. Each subplot displays results from the hyperparameter tuning procedure based on 5000 Monte-Carlo simulations using all 84 climate- and landscape attributes. (a) the red X marks the final model selected for subsequent analyses.

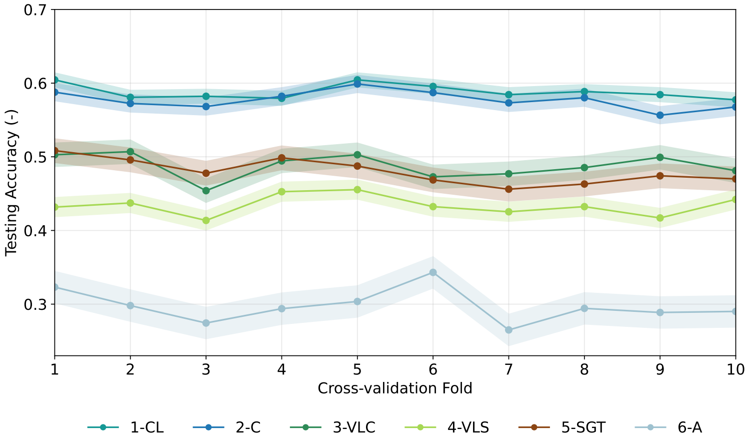

Figure S5. Testing accuracy across the 10-fold cross-validation for each of the six experiments. Each line connects the fold-specific testing accuracies (shown as dots), and the shaded area represents the standard deviation across folds, illustrating the variability in model performance within each experiment.

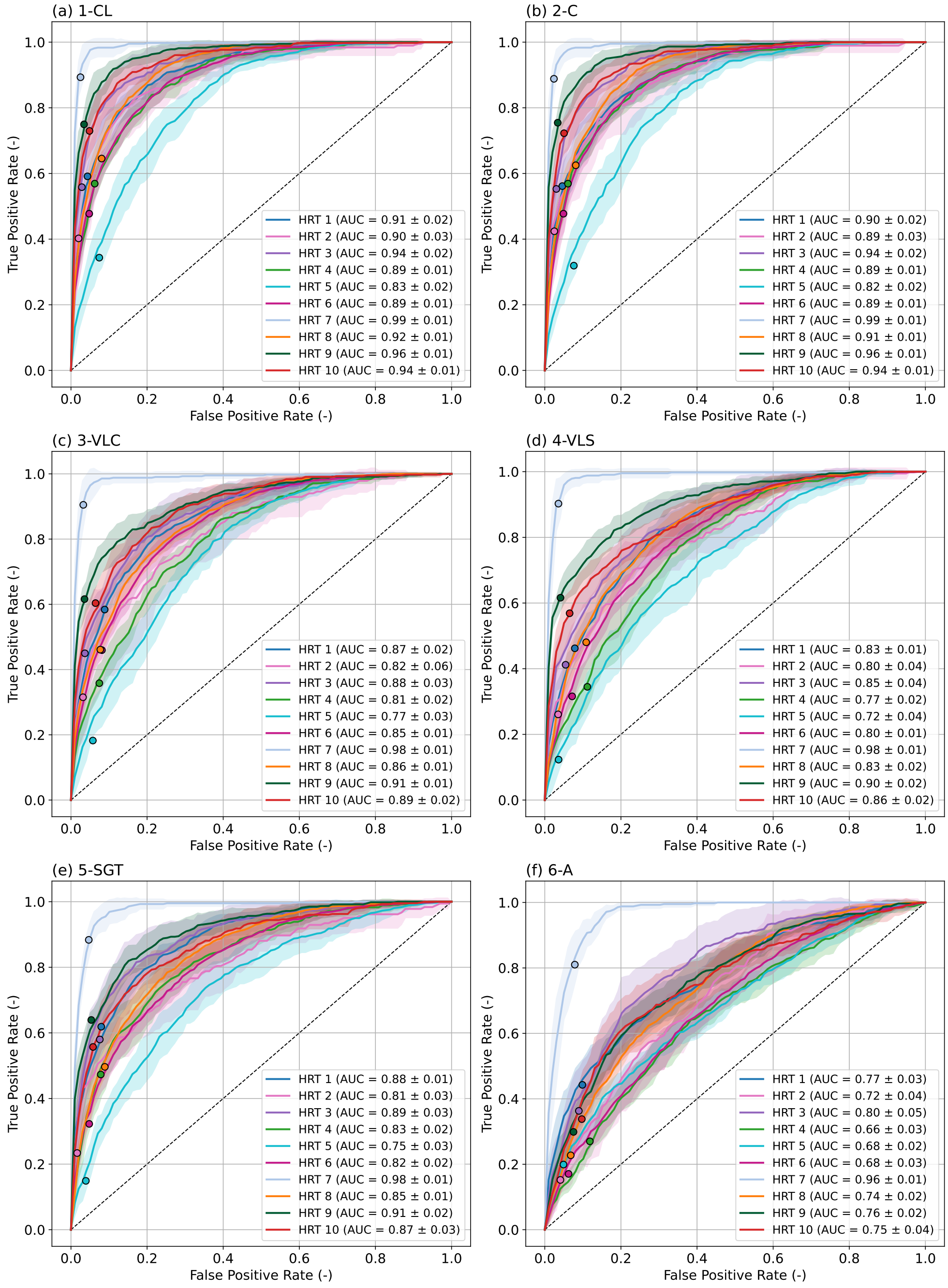

Figure S6. ROC curves for each experiment, showing one micro-averaged curve per hydrological response type (HRT) across all 10 cross-validation folds. Each curve illustrates the trade-off between true positive rate (T_{PR}) and false positive rate (F_{PR}) across probability thresholds. The filled circle on each curve indicates the T_{PR} and F_{PR} at the actual classification threshold used for final predictions. The dashed diagonal line represents random classification, and the area under each curve (A_{UC}) quantifies overall classification performance, with larger A_{UC} values indicating higher accuracy.

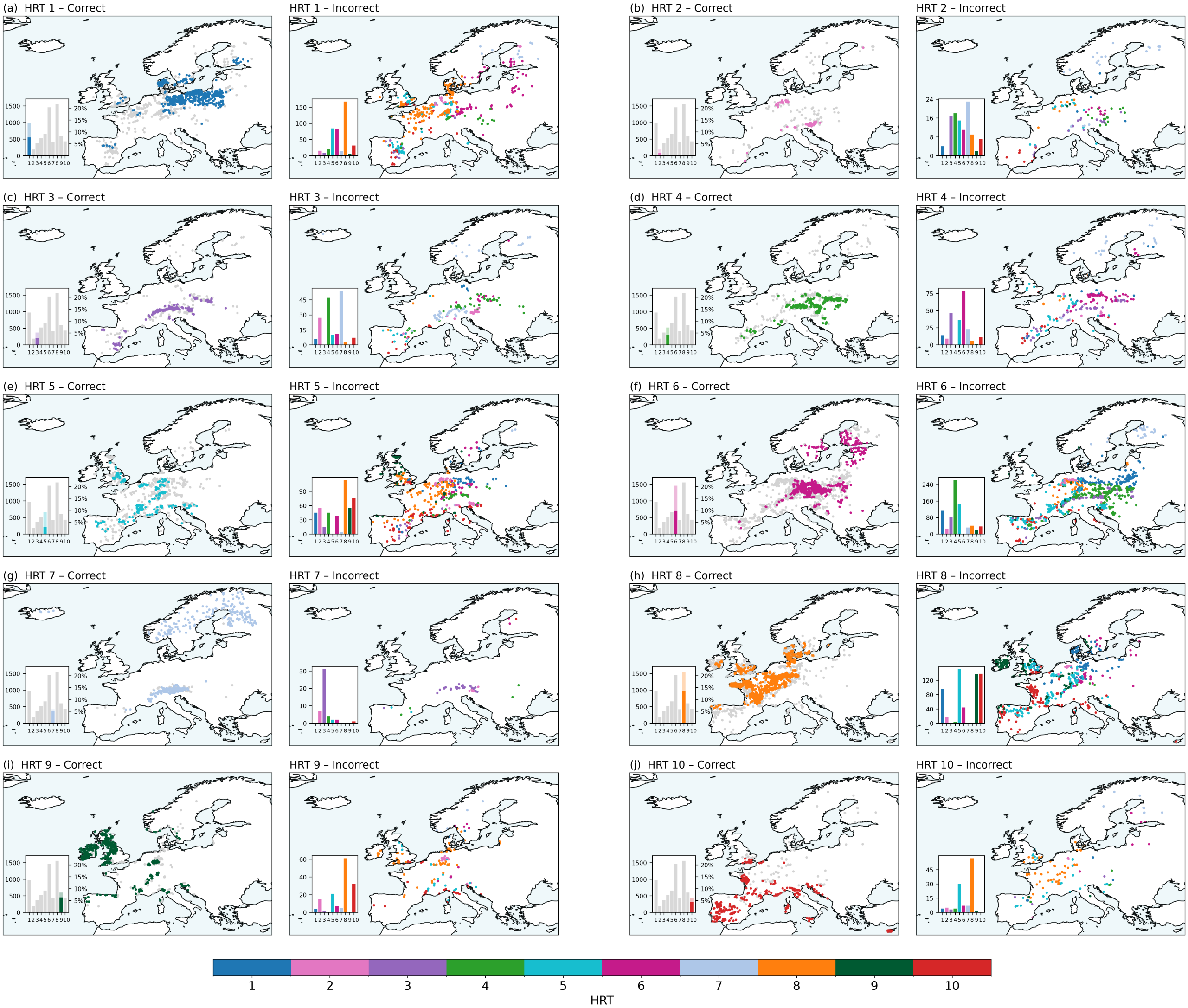

(a) HRT 1 – Correct

HRT 1 – Incorrect

(b) HRT 2 – Correct

HRT 2 – Incorrect

(c) HRT 3 – Correct

HRT 3 – Incorrect

(d) HRT 4 – Correct

HRT 4 – Incorrect

(e) HRT 5 – Correct

HRT 5 – Incorrect

(f) HRT 6 – Correct

HRT 6 – Incorrect

(g) HRT 7 – Correct

HRT 7 – Incorrect

(h) HRT 8 – Correct

HRT 8 – Incorrect

(i) HRT 9 – Correct

HRT 9 – Incorrect

(j) HRT 10 – Correct

HRT 10 – Incorrect

Figure S7. Maps showing correct and incorrect classification results for experiment 2-C. In the “correct” panels, only correctly classified catchments are shown in their cluster colours, while incorrectly classified catchments appear in grey. In the “incorrect” panels, only the misclassified catchments are displayed and coloured according to their *true* cluster, allowing visual assessment of which clusters are most frequently misclassified.

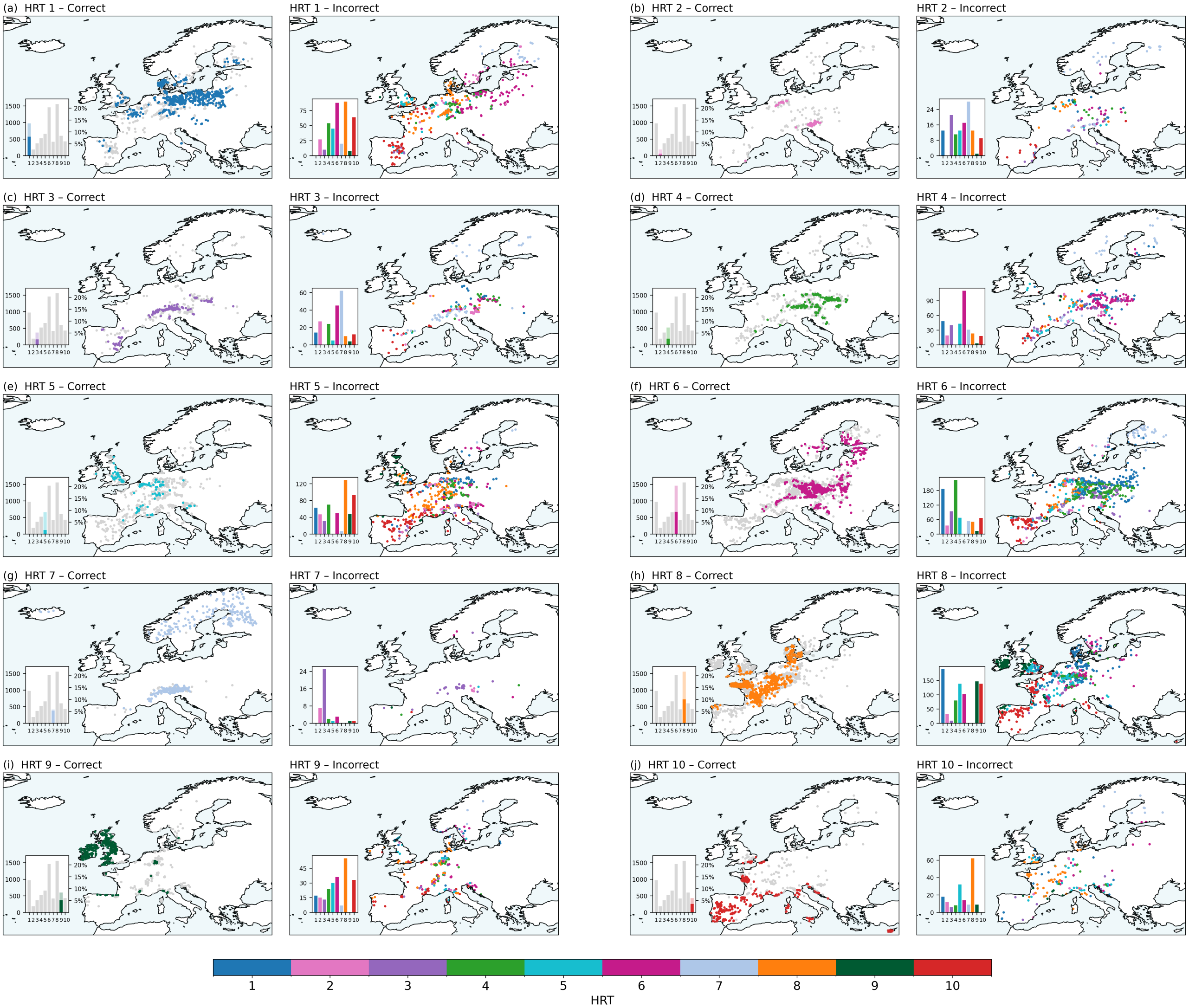
(a) HRT 1 – Correct
HRT 1 – Incorrect
(b) HRT 2 – Correct
HRT 2 – Incorrect
(c) HRT 3 – Correct
HRT 3 – Incorrect
(d) HRT 4 – Correct
HRT 4 – Incorrect
(e) HRT 5 – Correct
HRT 5 – Incorrect
(f) HRT 6 – Correct
HRT 6 – Incorrect
(g) HRT 7 – Correct
HRT 7 – Incorrect
(h) HRT 8 – Correct
HRT 8 – Incorrect
(i) HRT 9 – Correct
HRT 9 – Incorrect
(j) HRT 10 – Correct
HRT 10 – Incorrect

Figure S8. Maps showing correct and incorrect classification results for experiment 3-VLC. In the “correct” panels, only correctly classified catchments are shown in their cluster colours, while incorrectly classified catchments appear in grey. In the “incorrect” panels, only the misclassified catchments are displayed and coloured according to their *true* cluster, allowing visual assessment of which clusters are most frequently misclassified.

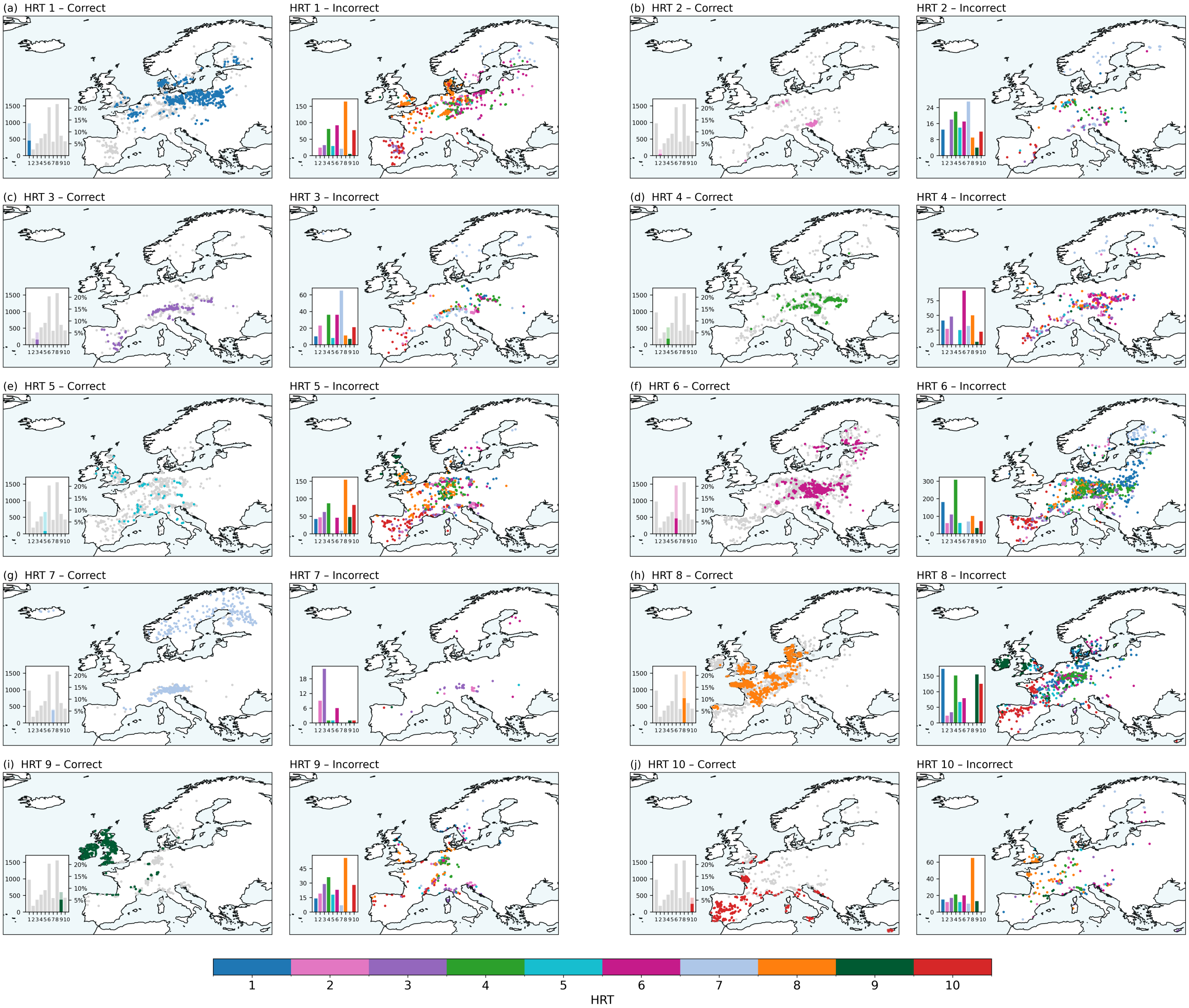

Figure S9. Maps showing correct and incorrect classification results for experiment 4-VLS. In the "correct" panels, only correctly classified catchments are shown in their cluster colours, while incorrectly classified catchments appear in grey. In the "incorrect" panels, only the misclassified catchments are displayed and coloured according to their *true* cluster, allowing visual assessment of which clusters are most frequently misclassified.

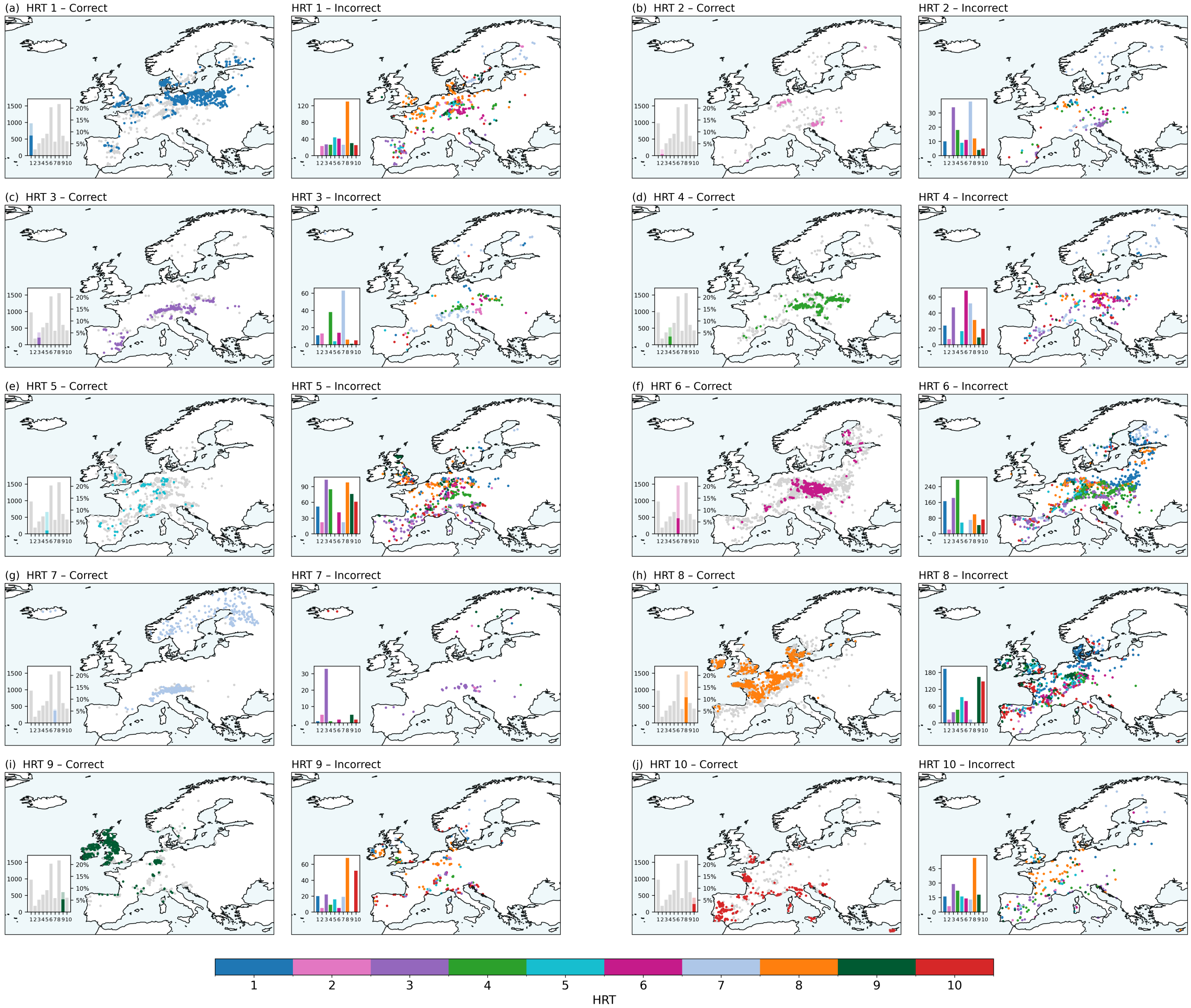

Figure S10. Maps showing correct and incorrect classification results for experiment 5-SGT. In the “correct” panels, only correctly classified catchments are shown in their cluster colours, while incorrectly classified catchments appear in grey. In the “incorrect” panels, only the misclassified catchments are displayed and coloured according to their *true* cluster, allowing visual assessment of which clusters are most frequently misclassified.

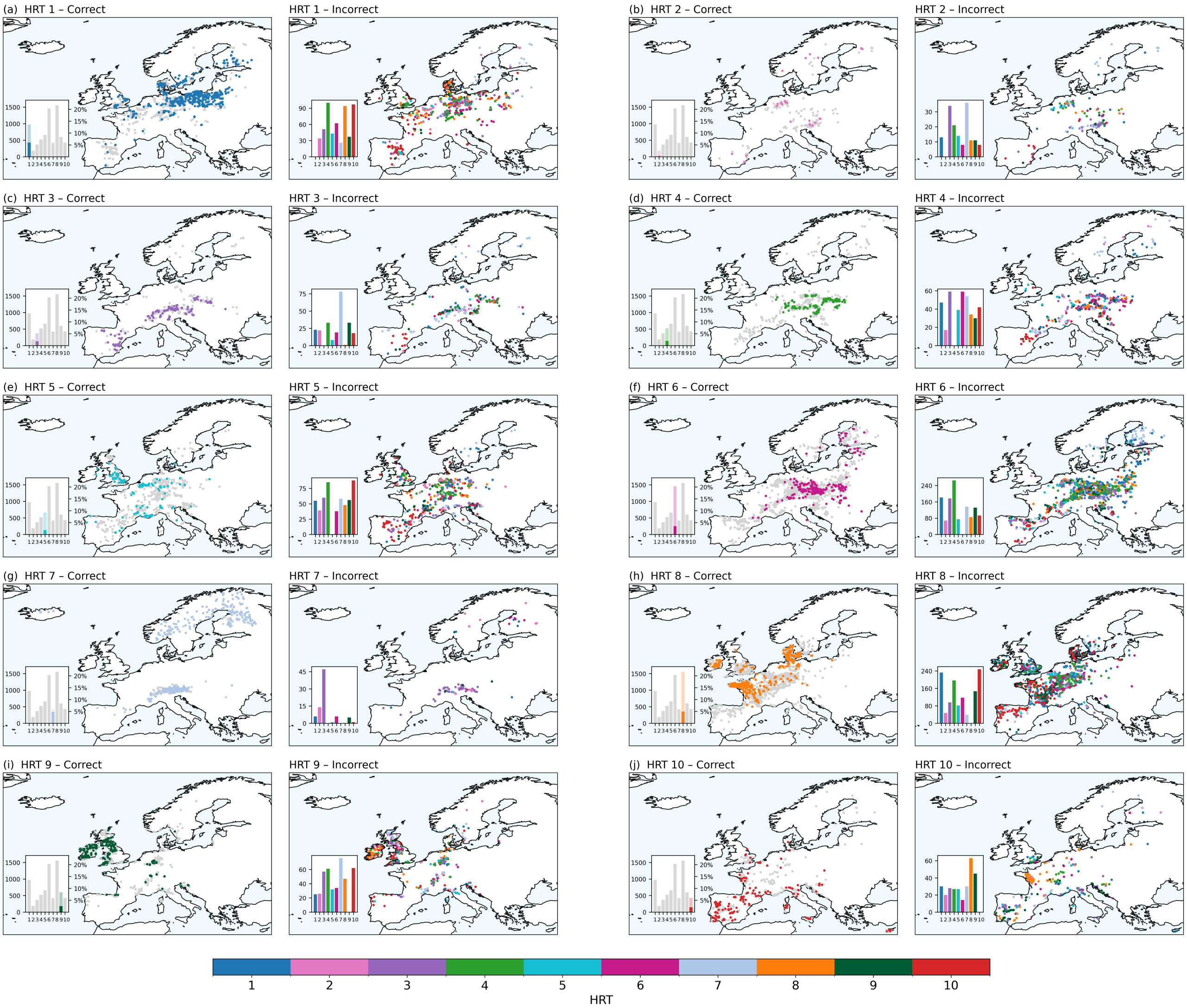

Figure S11. Maps showing correct and incorrect classification results for experiment 6-A. In the “correct” panels, only correctly classified catchments are shown in their cluster colours, while incorrectly classified catchments appear in grey. In the “incorrect” panels, only the misclassified catchments are displayed and coloured according to their *true* cluster, allowing visual assessment of which clusters are most frequently misclassified.

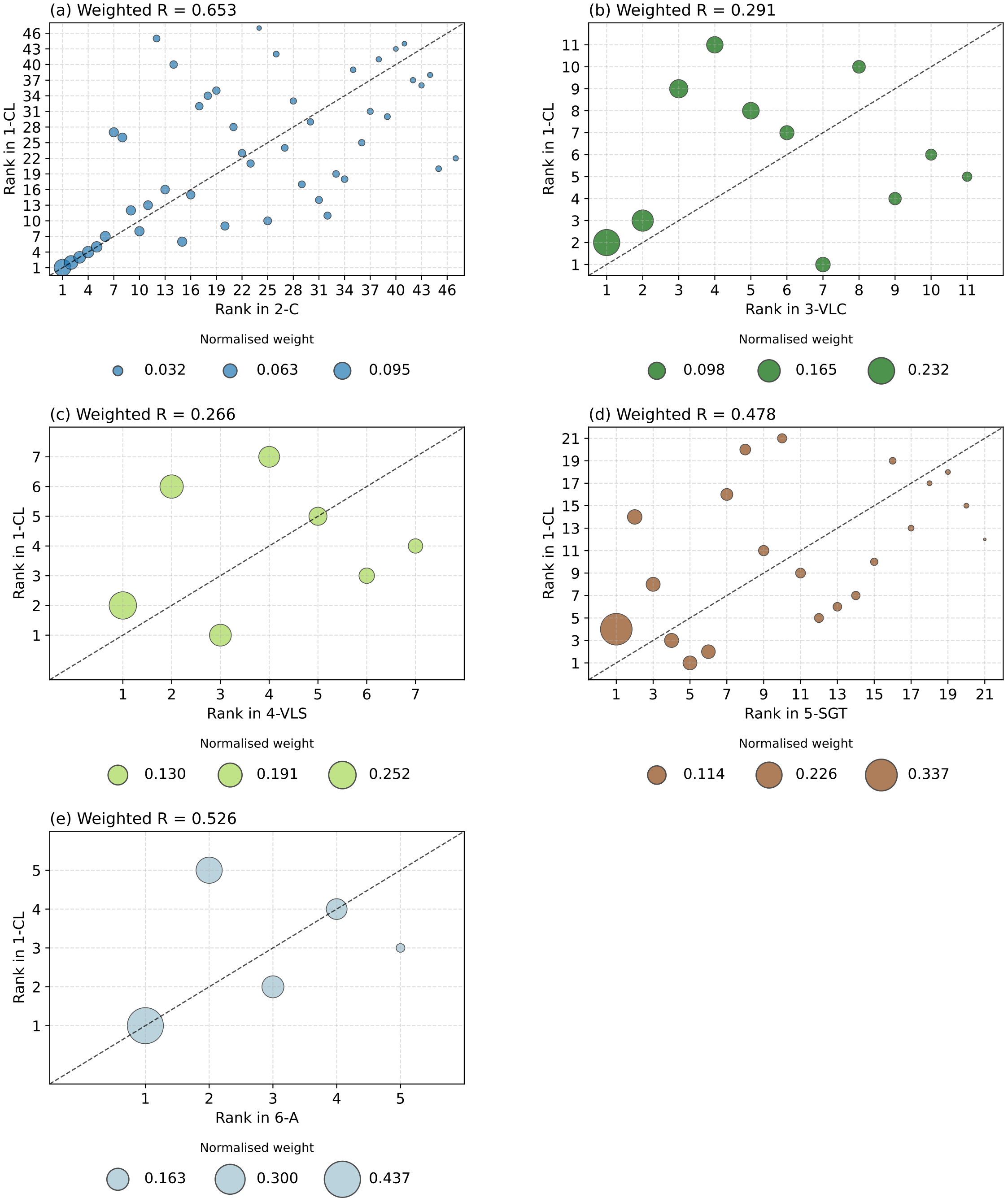

Figure S12. The feature importance rankings across five experiments. For each experiment, features were ranked based on their importance within that experiment and compared to their relative ranking in the full experiment (1-CL). Marker size represents the weighted correlation of feature importance between the experiment and 1-CL. For example, in panel (b), the ranking of signatures in experiment 3-VLC is shown relative to their position in 1-CL: the highest-ranking feature in 3-VLC that appears first in the 1-CL ranking is assigned rank 1. This visualisation highlights the consistency of feature importance across experiments.

References

Baker, D. B., Richards, R. P., Loftus, T. T., and Kramer, J. W.: A new flashiness index: Characteristics and applications to Midwestern rivers and streams, Journal of the American Water Resources Association, 40, 503–522, https://doi.org/10.1111/J.1752-1688.2004.TB01046.X, 2004.

Berghuijs, W. R., Hale, K., and Beria, H.: Technical note: Streamflow seasonality using directional statistics, Hydrol. Earth Syst. Sci, 29, 2851–2862, https://doi.org/10.5194/hess-29-2851-2025, 2025.

Bergstrom, S.: THE DEVELOPMENT OF A SNOW ROUTINE FOR THE HBV-2 MODEL, Hydrology Research, 6, 73–92, https://doi.org/10.2166/NH.1975.0006, 1975.

Blöschl, G., Sivapalan, M., Wagener, T., Viglione, A., and Savenije, H.: Runoff Prediction in Ungauged Basins: Synthesis across Processes, Places and Scales, Cambridge University Press, Cambridge, https://doi.org/DOI: 10.1017/CBO9781139235761, 2013.

Blöschl, G., Hall, J., Parajka, J., Perdigão, R. A. P., Merz, B., Arheimer, B., Aronica, G. T., Bilibashi, A., Bonacci, O., Borga, M., Čanjevac, I., Castellarin, A., Chirico, G. B., Claps, P., Fiala, K., Frolova, N., Gorbachova, L., Gül, A., Hannaford, J., Harrigan, S., Kireeva, M., Kiss, A., Kjeldsen, T. R., Kohnová, S., Koskela, J. J., Ledvinka, O., Macdonald, N., Mavrova-Guirguinova, M., Mediero, L., Merz, R., Molnar, P., Montanari, A., Murphy, C., Osuch, M., Ovcharuk, V., Radevski, I., Rogger, M., Salinas, J. L., Sauquet, E., Šraj, M., Szolgay, J., Viglione, A., Volpi, E., Wilson, D., Zaimi, K., and Živković, N.: Changing climate shifts timing of European floods, Science, 357, 588–590, https://doi.org/10.1126/science.aan2506, 2017.

Euser, T., Winsemius, H. C., Hrachowitz, M., Fenicia, F., Uhlenbrook, S., and Savenije, H. H.: A framework to assess the realism of model structures using hydrological signatures, Hydrology and Earth System Sciences, 17, 1893–1912, https://doi.org/10.5194/HESS-17-1893-2013, 2013.

Gao, H., Ding, Y., Zhao, Q., Hrachowitz, M., and Savenije, H. H.: The importance of aspect for modelling the hydrological response in a glacier catchment in Central Asia, Hydrological Processes, 31, 2842–2859, https://doi.org/10.1002/HYP.11224, 2017.

Hargreaves, G. H. and Samani, Z. A.: Estimating Potential Evapotranspiration, Journal of the Irrigation and Drainage Division, 108, 225–230, https://doi.org/10.1061/JRCEA4.0001390, 1982.

Ladson, A. R., Brown, R., Neal, B., and Nathan, R.: A Standard Approach to Baseflow Separation Using The Lyne and Hollick Filter, Australasian Journal of Water Resources, 17, 25–34, https://doi.org/10.7158/13241583.2013.11465417, 2013.

Parajka, J., Kohnová, S., Bálint, G., Barbuc, M., Borga, M., Claps, P., Cheval, S., Dumitrescu, A., Gaume, E., Hlavčová, K., Merz, R., Pfaundler, M., Stancalie, G., Szolgay, J., and Blöschl, G.: Seasonal characteristics of flood regimes across the Alpine–Carpathian range, Journal of Hydrology, 394, 78–89, https://doi.org/10.1016/J.JHYDROL.2010.05.015, 2010.

Pelletier, J. D., Broxton, P. D., Hazenberg, P., Zeng, X., Troch, P. A., Niu, G. Y., Williams, Z., Brunke, M. A., and Gochis, D.: A gridded global data set of soil, intact regolith, and sedimentary deposit thicknesses for regional and global land surface modeling, Journal of Advances in Modeling Earth Systems, 8, 41–65, https://doi.org/10.1002/2015MS000526, 2016.

Sawicz, K., Wagener, T., Sivapalan, M., Troch, P. A., and Carrillo, G.: Catchment classification: empirical analysis of hydrologic similarity based on catchment function in the eastern USA, Hydrol. Earth Syst. Sci, 15, 2895–2911, https://doi.org/10.5194/hess-15-2895-2011, 2011.

Van Oorschot, F., Van Der Ent, R. J., Alessandri, A., and Hrachowitz, M.: Influence of irrigation on root zone storage capacity estimation, Hydrology and Earth System Sciences, 28, 2313–2328, https://doi.org/10.5194/hess-28-2313-2024, 2024.

Woods, R. A.: Analytical model of seasonal climate impacts on snow hydrology: Continuous snowpacks, Advances in Water Resources, 32, 1465–1481, https://doi.org/10.1016/J.ADVWATRES.2009.06.011, 2009.